# Development of Localized Arc Filament RF Plasma Actuators for High-Speed and High Reynolds Number Flow Control

J.-H. Kim, M. Nishihara, I.V. Adamovich, and M. Samimy*

*Department of Mechanical Engineering, The Ohio State University*
*GDTL/AARL, 2300 West Case Rd., Columbus OH 43235-7531, USA*

S.V. Gorbatov and F.V. Pliavaka

*A.V. Lykov Heat and Mass Transfer Institute of National Academy of Sciences of Belarus*
*15 P. Brovka St., Minsk, 220072, Belarus*

***Corresponding author, samimy.1@osu.edu**

# Report Documentation Page

*Form Approved*
*OMB No. 0704-0188*



| 1. REPORT DATE | 2. REPORT TYPE | 3. DATES COVERED |
|---|---|---|
| **2010** | | **00-00-2010 to 00-00-2010** |

| 4. TITLE AND SUBTITLE | 5a. CONTRACT NUMBER |
|---|---|
| **Development of Localized Arc Filament RF Plasma Actuators for High-Speed and High Reynolds Number Flow Control** | 5b. GRANT NUMBER |
| | 5c. PROGRAM ELEMENT NUMBER |
| 6. AUTHOR(S) | 5d. PROJECT NUMBER |
| | 5e. TASK NUMBER |
| | 5f. WORK UNIT NUMBER |
| 7. PERFORMING ORGANIZATION NAME(S) AND ADDRESS(ES) **Ohio State University,Department of Mechanical Engineering,2300 West Case Rd,Columbus ,OH,43235** | 8. PERFORMING ORGANIZATION REPORT NUMBER |
| 9. SPONSORING/MONITORING AGENCY NAME(S) AND ADDRESS(ES) | 10. SPONSOR/MONITOR'S ACRONYM(S) |
| | 11. SPONSOR/MONITOR'S REPORT NUMBER(S) |

12. DISTRIBUTION/AVAILABILITY STATEMENT
**Approved for public release; distribution unlimited**

13. SUPPLEMENTARY NOTES
**accepted for publication in Experiments in Fluids**

14. ABSTRACT
**see report**

15. SUBJECT TERMS

| 16. SECURITY CLASSIFICATION OF: | | | 17. LIMITATION OF ABSTRACT | 18. NUMBER OF PAGES | 19a. NAME OF RESPONSIBLE PERSON |
|---|---|---|---|---|---|
| a. REPORT **unclassified** | b. ABSTRACT **unclassified** | c. THIS PAGE **unclassified** | **Same as Report (SAR)** | **23** | |

## Abstract

Recently developed Localized Arc Filament Plasma Actuators (LAFPAs) have shown tremendous control authority in high-speed and high Reynolds number flow for mixing enhancement and noise mitigation. Previously, these actuators were powered by a high voltage pulsed DC plasma generator with low energy coupling efficiency of 5-10%. In the present work, a new custom-designed 8-channel pulsed radio frequency (RF) plasma generator has been developed to power up to 8 plasma actuators operated over a wide range of forcing frequencies (up to 50 kHz) and duty cycles (1-50%), and at high energy coupling efficiency (up to 80-85%). This reduces input electrical power requirements by approximately an order of magnitude, down to 12 W per actuator operating at 10% duty cycle. The new pulsed RF plasma generator is scalable to a system with a large number of channels. Performance of pulsed RF plasma actuators used for flow control was studied in a Mach 0.9 circular jet with a Reynolds number of about 623,000 and compared with that of pulsed DC actuators. Eight actuators were distributed uniformly on the perimeter of a 2.54 cm diameter circular nozzle extension. Both types of actuators coupled approximately the same amount of power to the flow, but with drastically different electrical inputs to the power supplies. Particle image velocimetry measurements showed that jet centerline Mach number decay produced by DC and RF actuators operating at the same forcing frequencies and duty cycles is very similar. At a forcing Strouhal number near 0.3, close to the jet column instability frequency, well-organized periodic structures, with similar patterns and dimensions, were generated in the jets forced by both DC and RF actuators. Far-field acoustic measurements demonstrated similar trends in the Overall Sound Pressure Level (OASPL) change produced by both types of actuators, resulting in OASPL reduction up to 1.2-1.5 dB in both cases. We conclude that pulsed RF actuators demonstrate flow control authority similar to pulsed DC actuators, with a significantly reduced power budget.

## 1. Introduction

High-speed flow control by plasmas remains a rapidly growing research field with considerable literature. Potential plasma flow control applications include boundary layer transition and separation control, mixing enhancement, noise mitigation, suppressing cavity tones, shock-boundary layer interaction control, shock modification, and drag reduction. In the absence of strong magnetic field, two principal mechanisms of plasma flow control, both extensively studied in the literature, are Joule heating of the flow and electrohydrodynamic (EHD) flow entrainment by momentum transfer from charged species accelerated by Coulomb force. An extensive review of applications of the EHD mechanism in dielectric barrier discharge (DBD) and corona discharge plasma actuators for low-speed flow control is given by Moreau (2007). Recent results (Roupassov et al. 2009), which appear to extend applicability of DBD plasma actuators to high-speed flows of Mach 0.7-0.8, suggest that the effect of rapid Joule heating by the repetitively pulsed low-temperature plasma is dominant over that of a relatively weak EHD force interaction. The main implication of these results is that the use of repetitive rapid localized heating, which occurs both in high-temperature plasmas (such as arc filaments) and in low-temperature plasmas (such as in nanosecond pulse discharges), may well be the most effective common approach to high-speed flow control.

It has long been known that high-energy spark discharges and pulsed optical breakdown can generate strong shock waves in the surrounding air. Recent studies of arc discharge plasmas and laser-induced breakdown interaction with high-speed flows demonstrated that localized heating of the flow by a high-temperature plasma can significantly affect the flow, generating shocks, inducing flow separation, and producing large-scale structures (Leonov and Yarantsev 2008; Adelgren et al. 2005a; Adelgren et al. 2005b). These high-amplitude perturbations, induced by high-power electric discharges or lasers pulsed at a high repetition rate, may be used to control the high-speed flow field. Furthermore, this also suggests that if the forcing frequency (i.e. pulse repetition rate) is tuned to match one of the flow instability frequencies, a seeded perturbation with sufficiently high amplitude may be significantly amplified by the flow. Using this approach, considerable flow control authority may well be achieved using relatively low-power plasma actuators. The effect may be enhanced further by locating a perturbation source (i.e. a plasma actuator) near the point of maximum flow receptivity, and using multiple individually controlled actuators. This would enable control of both the forcing frequency and the phase, and would allow selective excitation of various flow instability modes (Samimy et al. 2007b).

Selection of actuators with suitable forcing characteristics is critical for effective flow control. In active control of jets and free shear layers, actuators are used to seed perturbations into the flow. The seeded perturbations may be either amplified or decayed, depending on their characteristics and flow instabilities. The actuator requirements depend on flow instability frequencies as well as on background noise level of the flow. In high-speed and high Reynolds number flows, actuators need to have both high bandwidth and high amplitude since frequencies associated with flows instabilities are high and so is the background noise. For this reason, using mechanical and piezoelectric actuators to excite instabilities in high-speed flows is problematic due to their low forcing frequency (for mechanical actuators) and low forcing amplitude (for piezo actuators).

Formation and development of large-scale structures in the shear layer of a circular jet involve three instability modes. The first is the initial shear layer instability (K-H type) due to the

velocity profile with an inflection point, which is present in the shear layer. The frequency of this instability mode, $f_0$, scales with the boundary layer momentum thickness at the nozzle exit, $\theta_0$, and ranges from $St_\theta = f_0\theta_0/U_j = 0.01$ to 0.02. The second is the jet column instability due to interaction between the flow structures and the jet plume. Since the size of flow structures near the end of the potential core is comparable to the nozzle exit diameter, the frequency of this instability mode is scaled with the nozzle exit diameter (D). The jet column is generally known to be unstable at $St_D = f_pD/U_j$ =0.2-0.6. The last instability in a circular jet is the azimuthal mode. In our previous flow control studies using plasma actuators, it was demonstrated that the noise and flow fields in circular Mach 0.9 jets (Samimy et al. 2007a; Kim et al. 2009) and Mach 1.3 jets (Samimy 2007b, Kim et al. 2008; Kim and Samimy 2009) are significantly affected by the choice of azimuthal mode at a fixed forcing frequency.

Recent experiments at The Ohio State University demonstrated that localized arc filament plasma actuators (LAFPAs) are capable of generating high-amplitude perturbations at a relatively low plasma power and can be operated at high forcing frequencies, up to ~100 kHz (Samimy et al. 2007a; Samimy et al. 2007b; Kim et al. 2009). These actuators have been used to generate localized heating in atmospheric pressure, high-speed jet flows (Mach=0.9-1.65). The results show that significant effect on the flow field, as well as considerable jet noise reduction are achieved at the plasma power of about 0.5% of the flow power, $\dot{m}\left(c_pT_0 + U_j^2/2\right)$, which demonstrates significant potential for the use of this approach in large-scale flows. The distance between the two electrodes of an actuator is fixed and so is the generated disturbance level, which is controlled by breakdown of air between the electrodes. Therefore, the number of actuators will scale with the jet diameter, which will make the control technique more energy efficient in larger scales.

Most experiments using LAFPAs (Samimy et al. 2004; Samimy et al. 2007a; Samimy et al. 2007b; Utkin et al. 2007) have been conducted using up to 8 plasma actuators distributed along the circumference of a 1 inch (2.54 cm) diameter nozzle near the exit plane, although some limited results have been obtained in a Mach 1.3 rectangular jet with a cross section of 0.5 in x 1/5 inch (1.27 cm x 3.81 cm) (Utkin et al. 2007; Adamovich et al. 2009). Preliminary scaling studies (Samimy et al. 2006) have also been conducted in a 7.5 inch (19.05 cm) diameter jet using 32 actuators (simple scaling of the number of actuators with the jet diameter would require 60 actuators). Similar trends have been observed in axial growth of initial perturbations generated by the actuators in a 1 inch Mach 0.84 jet and in a 7.5 inch Mach 0.5 jet, which appears very promising. However, perturbation growth in a 7.5 inch jet at Mach 0.9 was diminished, which was attributed to a smaller ratio of the number of actuators to nozzle circumference than in the 1 inch diameter jet. Also, experiments in a 7.5 inch jet were constrained to using a limited number of azimuthal forcing modes since the plasma generator controlling 32 actuators had only 8 independent channels, and therefore groups of 4 actuators had to be powered at the same time.

Further development of localized arc filament plasma actuator technology, its optimization and scaling, and applicability to large-scale flows would require highly energy-efficient, lightweight, multi-channel (a few tens to a few hundred channels) pulsed plasma generators with independent control of individual actuators or small actuator groups. Assuming that the number of actuators required for efficient flow control scales linearly with jet diameter (note that the flow power scales as diameter squared), controlling a 12 inch diameter jet would require the use of at least ~100 actuators. Expanding an 8-channel pulsed DC plasma generator used in our previous studies (Samimy et al. 2007a; Samimy et al. 2007b; Utkin et al. 2007) to a

large number of channels appears impractical due to excessively high power consumption. In this plasma generator, very low fraction of DC power is coupled to the actuators (5-10%), with the rest of the power dissipated in massive ballast resistors acting as heat sinks. This occurs because producing breakdown between the actuator electrodes requires high voltage (5-10 kV), while after breakdown the voltage across the arc discharge filament is much lower, typically a few hundred Volts.

In our previous work (Adamovich et al. 2009), we studied the feasibility of the use of pulsed radio frequency (RF) plasma generators with high energy conversion efficiency. These preliminary results demonstrated that pulsed RF plasma actuators produce rapid localized heating in a Mach 0.9 flow up to high temperatures, T=1200-2500$^0$ C. Also, qualitative flow visualization have shown that Mach 0.9 flow forcing by two pulsed RF actuators results in generating large-scale periodic structures, similar to structures produced by two pulsed DC actuators operated at the same frequency and same actuator power. This suggests that the use of pulsed RF actuator arrays may provide significant flow control authority, at a much lower input electrical power (up to an order of magnitude less compared to pulsed DC actuators). On the other hand, RF plasma temperatures were found to be significantly higher than DC plasma temperatures, by up to 1000-1500$^0$ C (Adamovich et al. 2009). Since in both types of actuators flow forcing is induced by localized Joule heating, their quantitative effect on the flow may well be different. Therefore, quantitative comparison of the effect of RF and DC plasma actuators on the flow field and jet noise in a wide range of forcing parameters is necessary.

The objectives of the present work are to characterize a new 8-channel pulsed RF plasma generator and compare it quantitatively with the 8-channel pulsed DC generator used in our previous work, as well as to compare the performance of the two systems in controlling a Mach 0.9 circular jet with a Reynolds number of 623,000.

## 2. Experimental Facility and Techniques

The experiments were conducted in the Gas Dynamics and Turbulence Laboratory at The Ohio State University using ambient air compressed, dried, and stored in two tanks at a pressure of up to 16 MPa with a capacity of 36 m$^3$. Compressed air is supplied to the stagnation chamber of the high-speed jet facility before flowing through a convergent axisymmetric nozzle with an exit diameter (D) of 2.54 cm (1.0 in). A cylindrical nozzle extension, made of boron nitride ceramic, is attached to the nozzle exit to house eight plasma actuators. The jet flow exiting the

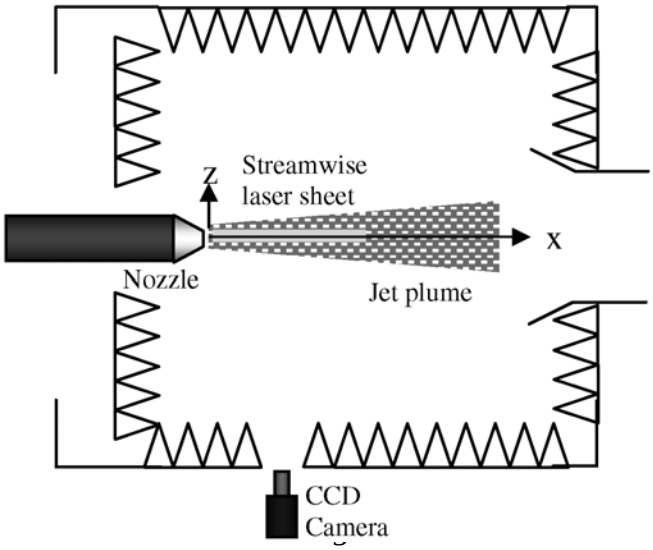


Fig. 1 Schematic of the jet flow and the PIV setup (not to scale). The *y* coordinate is normal to the *x*-*z* plane.

nozzle is discharged horizontally into an anechoic chamber, as shown schematically in Fig. 1. The Reynolds number of the jet based on the jet diameter is 623,000.

A two-component particle image velocimetry (PIV) system was used to measure the *x* and *y* velocity components in the *x*–*y* plane illuminated by a dual-head Spectra Physics PIV-400 Nd:YAG laser operating in the 2nd harmonic (see Fig. 1). Each laser head produced pulse energy of approximately 350 mJ/pulse. Images were acquired and processed by a LaVision PIV system using a 2000 by 2000 pixel Redlake CCD camera with a 75–300-mm Vivitar zoom lens. Image pairs were acquired at a sampling rate of approximately 5 Hz, with time delay between laser pulses in each pair of 2.0 µsec. The jet was seeded with di-ethyl-hexyl-sebacat fluid introduced 2.75 m upstream of the nozzle exit by a four-jet atomizer, to provide homogenous dispersion of the seed particles throughout the flow. Small amount of air, as well as fog from a fog generator, were also injected into a 15-inch (38 cm) diameter cylinder coaxial with the jet to generate a very low-speed fog-seeded co-flow (see Fig. 2). The camera captured streamwise laser sheet images (first ~ 10 jet diameters) orthogonally, as shown in Fig. 1. Spatial resolution of the resultant velocity field is approximately 2 mm. The uncertainty in the average velocity measured by PIV system is about 6%. Detailed description of the PIV diagnostics and data processing is given in our previous publications (Samimy et al. 2007a; Samimy et al. 2007b; Kim et al. 2009). Far-field overall sound pressure level (OASPL) was measured using two 1/4-in. diameter B&K microphones, located at $30^0$ and $90^0$ polar angles relative to the jet axis with a distance of 83 and 45 nozzle diameters from the nozzle exit, respectively. The microphones were calibrated using a 94-dB, 1-kHz sine wave. The frequency response of the microphones is flat up to 80 kHz. The uncertainty in OASPL is about 0.6 dB. Acoustic signal sampling, filtering, amplification, and normalization are discussed in greater detail in our previous work (Samimy et al. 2007a).

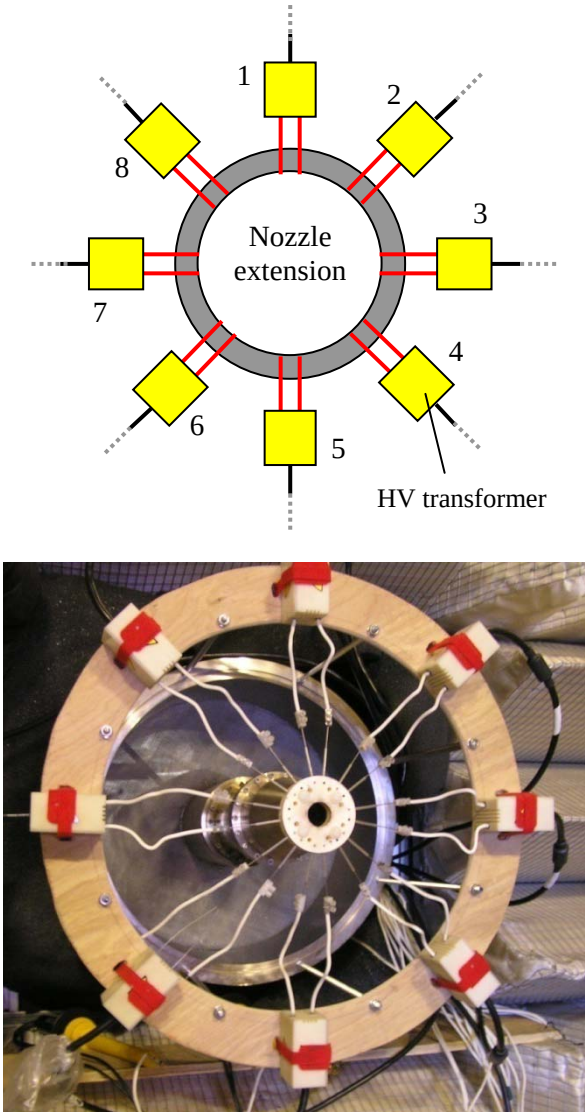


Fig. 2 Schematic and a photograph of nozzle extension with plasma actuators and high voltage transformers

A boron nitride ceramic nozzle extension, with the same internal diameter as the nozzle exit, is attached to the nozzle, as shown in Fig. 2. The extension is used to house eight pairs of 1 mm diameter pin electrodes made of tungsten wire, uniformly distributed around the perimeter. Each

electrode pair, with electrode spacing of 4 mm center-to-center, forms a plasma actuator. The center-to-center distance between electrodes of adjacent actuators is 6 mm. The electrodes are inserted into the extension through radial channels (see Fig. 2) and are housed in the ring-shaped groove 0.5 mm deep and 1 mm wide, located 1 mm from the exit plane of the nozzle extension. The groove improves plasma stability and prevents the plasma from being blown off by the flow. Tungsten has proved to be extremely resistant to erosion which may be caused by the high-temperature arc discharge between the electrodes. In the present experiments, electrode erosion in RF actuators was significantly reduced compared with that in DC actuators.

In our previous plasma flow control experiments (Samimy et al. 2007a; Samimy et al. 2007b), we used a custom-built 8-channel pulsed DC plasma generator with independent control of pulse repetition rate, duty cycle, and phase on individual channels, described in greater detail by Utkin et al. (2007). The pulsed DC generator has been extensively used for mixing enhancement and noise mitigation in 1 inch (2.54 cm) diameter Mach 0.9-1.65 jets. The most serious limitation of the DC plasma generator is its low efficiency. Only 5-10% of the output power is coupled to the flow and the rest is dissipated on ballast resistors. The use of high-power resistors also significantly increases the weight and size of the plasma generator and makes scaling to a large number of channels impractical. In the present work, we are using a custom-designed, 8-channel, pulsed RF plasma generator with electronic ballast, which has high power conversion efficiency. Feasibility of this approach has been tested in our recent work using two single-channel pulsed RF generators (Adamovich et al. 2009). The motivation for this approach is the development of multi-channel (~50-100 channels), highly energy efficient plasma generators with independent control of individual channels, which can be used for flow control and noise mitigation in a larger facility with an exit diameter of about 6 to12 inch (15-30 cm).

A schematic of a single channel of the 8-channel pulsed RF plasma generator is shown in Fig. 3. Eight parallel channels of the plasma generator are powered by a relatively low input DC voltage (400 V) from a high-current DC power supply (500 V, 20 A Magna-Power Electronics; 10 kV, 1 A Glassman; or 2 kV, 3A DEL) operated in a voltage stabilized mode. The input DC voltage is pulsed using a pair of fast response MOSFET (Metal-Oxide-Semiconductor Field

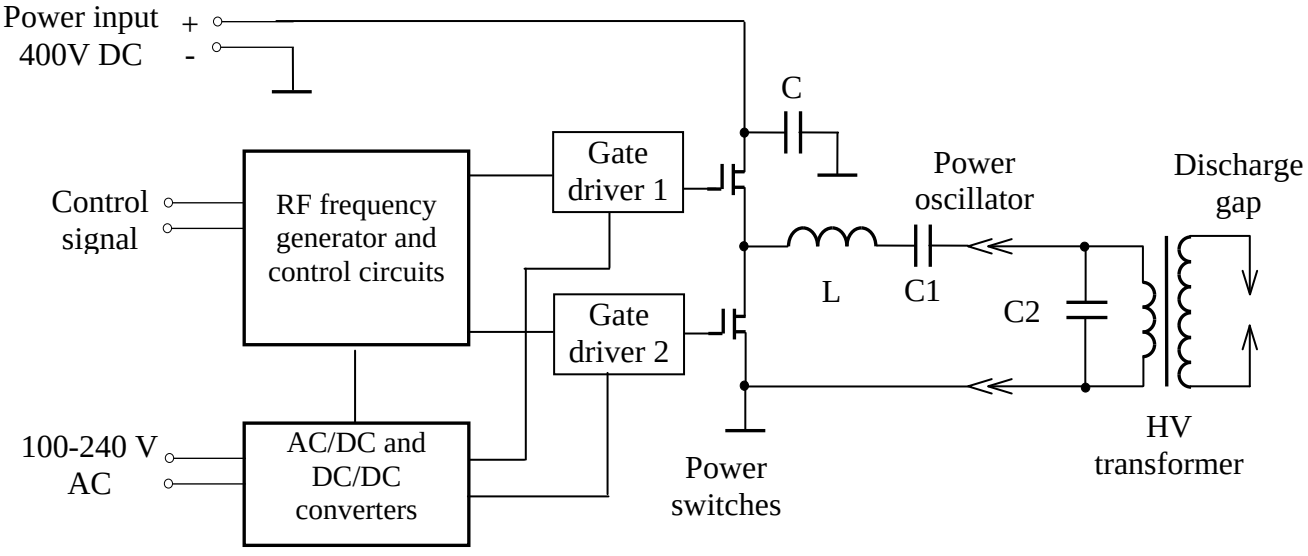


Fig. 3 Schematic of a single channel of the 8-channel pulsed RF plasma generator

Effect Transistor) power switches (see Fig. 3) operating out of phase at a carrier RF frequency of 1 MHz. This produces a burst of 400 V peak voltage rectangular pulses at a 1 MHz pulse repetition rate. The burst repetition rate, duration, and phase on individual channels are controlled by a 5 V rectangular pulse train produced by an 8-channel National Instruments digital-to-analog output PCI card and LabView software. The PCI card is galvanically isolated from the plasma generator circuit using digital isolators. The carrier frequency signal is generated internally, modulated using the step function input control signal, and boosted by gate drivers to operate MOSFET power switches (see Fig. 3). The carrier RF frequency signal generator / controller is incorporated into a Xilinx PLD (Programmable Logic Device) chip. The PLD configuration and generation parameters can be changed using a JTAG (Joint Test Action Group) programmer. The controller unit and the MOSFET drivers are powered by a DC/DC converter galvanically isolated from AC power input using a digital isolator (see Fig. 3).

The power converter is designed as a half-bridge push-pull circuit, which operates in two different modes during each pulse burst, "resonance" mode before breakdown and "current-limited" mode after breakdown is achieved between the discharge electrodes. The rise and fall time of the voltage at the discharge gap (Fig. 3) was significantly reduced with this approach. The fall time after breakdown was reduced by an order of magnitude when compared with that in the DC generator. In the resonance mode, the power converter operates as a pair of coupled oscillators. The resonance frequency of the $L$-$C_2$ oscillator is approximately $f = 1/\left(2\pi\sqrt{LC_2}\right) \approx 1$ MHz. Therefore driving this oscillator at the carrier frequency tuned to the resonance frequency produces voltage oscillations with rapidly rising amplitude, up to 20-25 kV over 2-3 periods (2-3 μsec). If the output voltage exceeds breakdown threshold, capacitor $C_2$ is shunted by an arc discharge filament generated in the flow between the electrodes, with low impedance, the resonance frequency becomes lower than the carrier frequency, $f = 1/\left(2\pi\sqrt{LC_1}\right) \approx 0.7$ MHz, and the circuit $Q$ factor significantly decreases. In this case, the arc current, ~0.2-0.4 A RMS, is controlled by the impedance of the $L$-$C_1$ oscillator, and the output voltage is greatly reduced to a few hundred Volts, resulting in power dissipation in the current-limited arc discharge of the order of 100 W RMS. As can be seen from Fig. 3, the circuit on the secondary side of the high voltage transformer and the load (plasma actuator) are not grounded during operation.

The weight of the pulsed RF plasma generator, including 8 high voltage transformers, is approximately 14 kg. Forced air cooling is used to cool power switches mounted on heat sinks. Power cables connecting the plasma generator with the main DC power supply and with external high-voltage transformers can be long, up to at least a few meters. On the other hand, the high-voltage transformers need to be placed relatively close to the load (i.e. plasma actuators), within 30-50 cm, since long electrode cables would increase the capacitance of the $L$-$C_1$ oscillator and therefore reduce the resonance frequency. The resonance frequency reduction would considerably increase voltage rise time and delay breakdown between the electrodes, which would preclude operation at high burst repetition rates. For this reason, in the present work the transformers were mounted on a 60 cm inner diameter ring support, as shown in Fig. 2.

During operation, the input DC current was measured by a LeCroy CP031 Hall effect current probe (100 MHz bandwidth, 3.5 nsec response time). The actuator voltage was determined as a difference between the potentials of two discharge electrodes measured simultaneously, using two high-voltage probes, Tektronix P6015A and Agilent Technology N2771A. In the present work, the bulk of actuator current measurements have been done using Tektronix AM503S Hall effect current probe system (15 MHz bandwidth, response time 23 ns) since the LeCroy current probe is not designed for the use in high-voltage (10 kV range) circuits.

Note that the actuator current rise time during breakdown is typically less than 10 nsec (see Section 3.1). For this reason, breakdown current and breakdown pulse energy cannot be measured accurately using the Tektronix current probe. Several high-resolution actuator current and breakdown pulse energy measurements have been done using a custom-designed, low inductance, low capacitance resistive current probe (response time several nsec) used in our previous work (Adamovich et al. 2009). However, these measurements require grounding one of the actuator electrodes, which may affect the resonance frequency of the power oscillator as well as increase EMI noise. During the present experiments, EMI noise from the plasma generator and the actuators was found to be fairly low and did not cause any interference problems with the diagnostics.

For a given burst repetition rate (forcing frequency), $f_F$, and duty cycle, $0<\delta<1$, the input control pulse train is given as follows,

$$g(t)=\begin{cases} 0 \quad if \quad 0<t<\dfrac{m\phi_a}{2\pi f_F} \\ 1 \quad if \quad \dfrac{m\phi}{2\pi f_F}<t<\dfrac{m\phi}{2\pi f_F}+\dfrac{\delta}{f_F} \\ 0 \quad if \quad \dfrac{m\phi}{2\pi f_F}+\dfrac{\delta}{f_F}<t<1 \end{cases} \tag{1}$$

where $\phi_a=\pi(i-1)/4$ is the channel phase corresponding to the azimuthal location of the actuator in the nozzle extension (see Fig. 2), $i=1, 2, \ldots, N$ is the channel number, $N$ is the number of channels ($N$=8 in the present work), and $m$ is the phase shift parameter (azimuthal mode number). For $m$=0, all channels (plasma actuators) operate in phase, producing axisymmetric forcing mode; $m$=1 produces sequential operation in the first helical mode; and $m$=±1 generates two counter-rotating helical modes, superposition of which produces a "flapping" mode. A more detailed description of the input pulse train is given in Samimy et al. (2007a) and Kim et al. (2009).

## 3. Results and Discussion

### *3.1. Actuator characterization*

Figure 4 shows typical plasma actuator voltage and current waveforms produced during a single RF burst in a Mach 0.9 jet, at a burst repetition rate (forcing frequency) of 3.5 kHz and 3.5% duty cycle (burst duration 10 μsec). It can be seen that in the beginning of the burst, the RF voltage rapidly increases up to 7 kV (over about 1 μsec), after which breakdown occurs between the electrodes (note significant current overshoot during breakdown, which is not completely resolved by the Tektronix current probe). After breakdown, both voltage and current are greatly reduced as the discharge transitions into the current-limited mode, oscillating at the RF carrier frequency of 1 MHz, with peak values of approximately 0.7 kV and 0.7 A, respectively. Although breakdown voltage somewhat varies burst-to-burst, voltage and current waveforms in the current-limited mode are reproduced well.

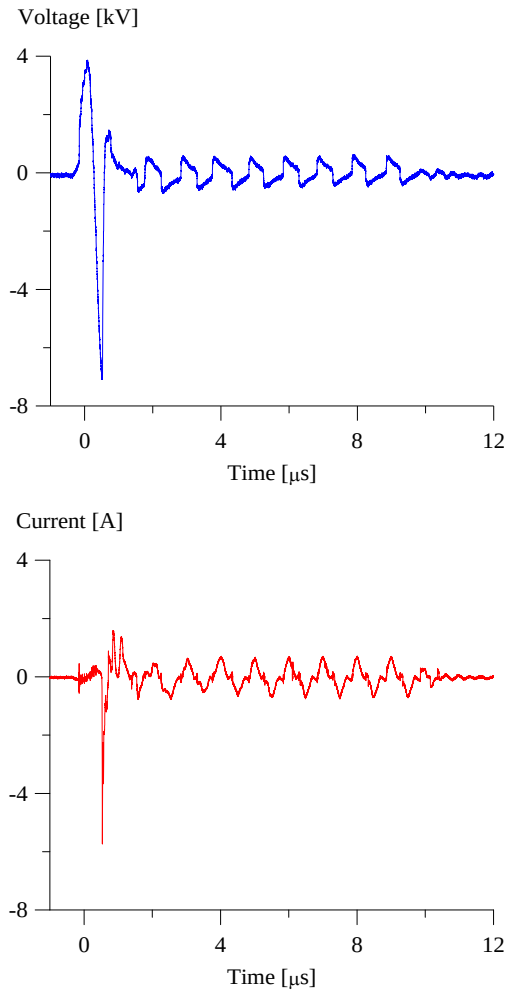


Fig. 4 Actuator voltage and current traces during a single burst at the forcing frequency of 3.5 kHz and 3.5% duty cycle in a Mach 0.9 jet.

The voltage, current, and power traces in a plasma actuator in a Mach 0.9 jet at a forcing frequency of 3.5 kHz and at a duty cycle of 5% (burst duration 14 μsec) are shown in Figs. 5 and 6 for during breakdown followed by the resonance mode and the current-limited mode, respectively. Note that the vertical scale in Figure 5 is significantly larger, to capture the entire range of voltage and current variation during breakdown. Current waveforms shown in Figs. 5 and 6 have been measured using a high bandwidth resistive current probe with response time of several nsec, and with one of the actuator electrodes grounded. It can be seen that voltage and current overshoot during breakdown (10 kV, 30 A) results in peak discharge power of about 80 kW. After breakdown, both voltage and current fall dramatically over a few tens of nanoseconds (see Fig. 5). The breakdown pulse energy, integrated over 40 nsec after breakdown is approximately 0.4 mJ. This is consistent with the breakdown pulse energy of 0.5 mJ, measured in quiescent air between two pin electrodes separated by a 3 mm gap. High peak power and pulse energy during breakdown are likely to be responsible for strong compression waves generated by both pulsed DC and pulsed RF arc discharges. In our previous work (Adamovich et al. 2009), multiple compression wave fronts were observed in schlieren images. Breakdown pulse energy measured both in a Mach 0.9 jet and in quiescent air demonstrates significant burst-to-burst variation, up to ±50%, mainly because breakdown voltage varies burst-to-burst. Extensive breakdown pulse energy measurements were also problematic

since they required grounding one of actuator electrodes, which may affect the resonance frequency of the power oscillator.

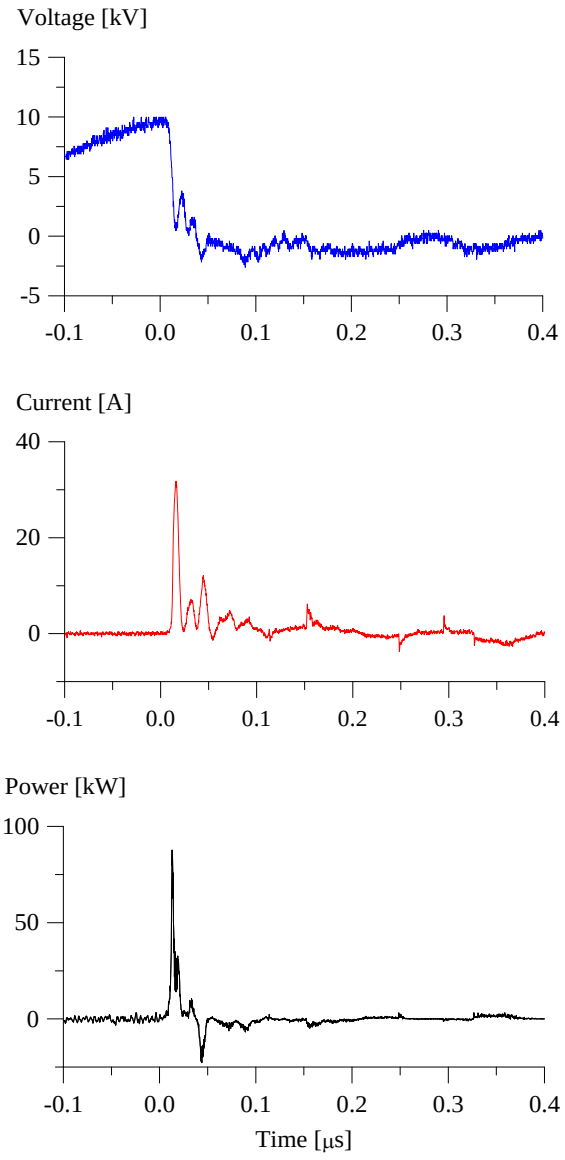


Fig. 5 Actuator voltage, current, and power traces during breakdown in a Mach 0.9 jet. Forcing frequency and duty cycle are 3.5 kHz and 5%, respectively. Peak power 80 kW, breakdown pulse energy 0.4 mJ.

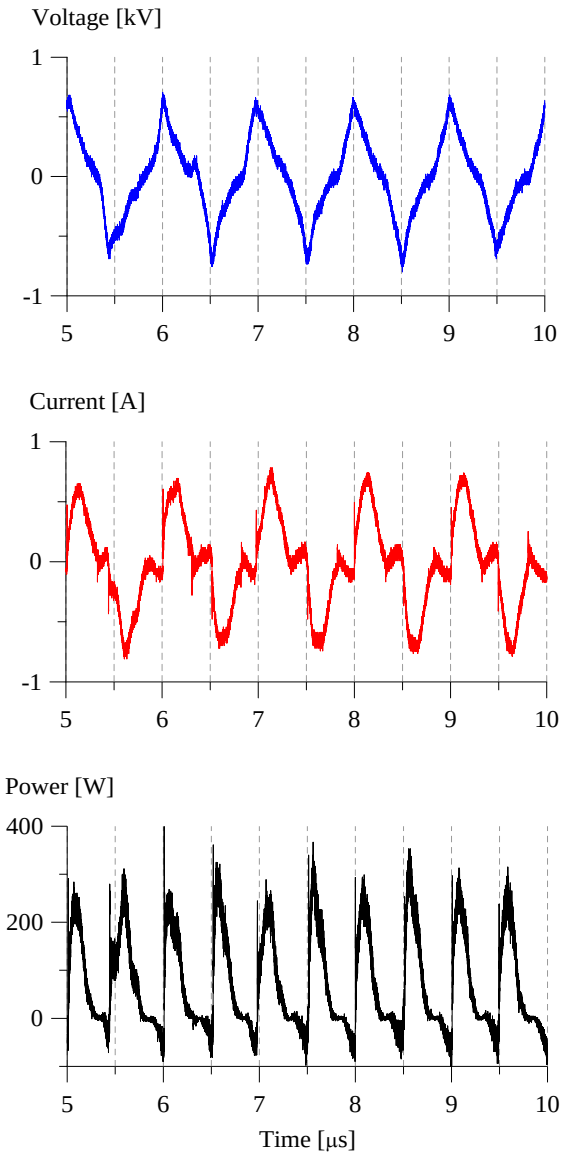


Fig. 6 Actuator voltage, current, and power in the current limited mode at the conditions of Figure 5. Average discharge power during the burst 70 W.

In the current-limited mode, voltage and current oscillate at 1 MHz nearly in phase (see Fig. 6), with peak voltage, current, and power values of approximately 0.7 kV, 0.7 A, and 300 W, respectively. The average discharge power in the current limited mode is approximately 0.07 mJ/µsec (70 W), which corresponds to the burst energy of approximately 0.7 mJ for the burst duration of 10 µs. This shows that for relatively short burst durations, ~5-20 µsec, breakdown pulse energy and the current-limited RF burst energy may be comparable. Neglecting the breakdown pulse energy gives the lower bound of the power dissipated in the actuator. The time-averaged actuator power, averaged over the waveform with multiple RF bursts is calculated by multiplying the burst energy by the forcing frequency. The lower bound, time-averaged actuator power for the conditions of Figs. 5 and 6 is 2.5 W (0.7 mJ x 3.5 kHz). Taking into account the breakdown pulse energy increases the time-averaged actuator power to 3.9 W, (0.4+0.7 mJ) x 3.5 kHz = 3.9 W. However, this power value has significant uncertainty, approximately ±20%, due to large burst-to-burst variation of the breakdown pulse energy, 0.4±0.2 mJ. For this reason, actuator power and efficiency calculations in the remainder of the present paper have been done without taking into account the breakdown pulse energy, and therefore represent lower bound values.

The present measurements show that the single actuator power in the current-limited mode is weakly affected by both burst duration (6-10 µsec) and forcing frequency (5-25 kHz). The use of a higher current DC power supply (2 kV, 3 A DEL or 500 V, 20 A Magna Power instead of 10 kV, 1 A Glassman) also considerably reduced input DC current oscillations during operation, as well as run-to-run actuator power variation. With a 3 A DC power supply, single actuator power remains within 0.09-0.10 mJ/µsec (90-100 W), with standard deviation of 3-5% percent for several different actuators tested. Therefore the actuator power averaged over the

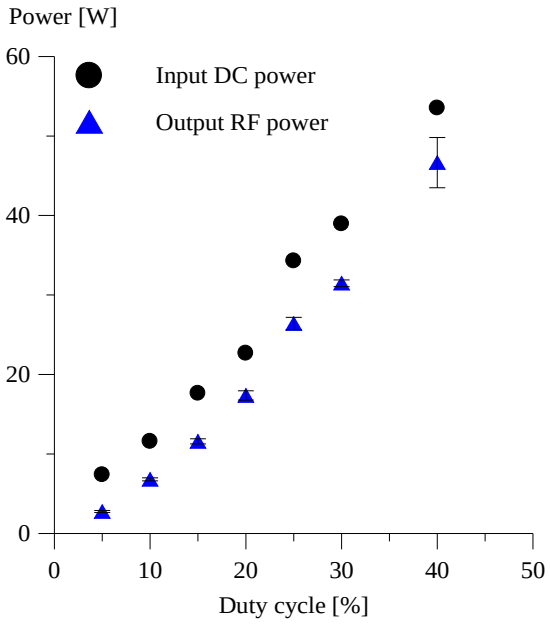


Fig. 7 Time-averaged input DC power and lower bound pulsed RF discharge power at a forcing frequency of 5 kHz vs. duty cycle. at Mach 0.9.

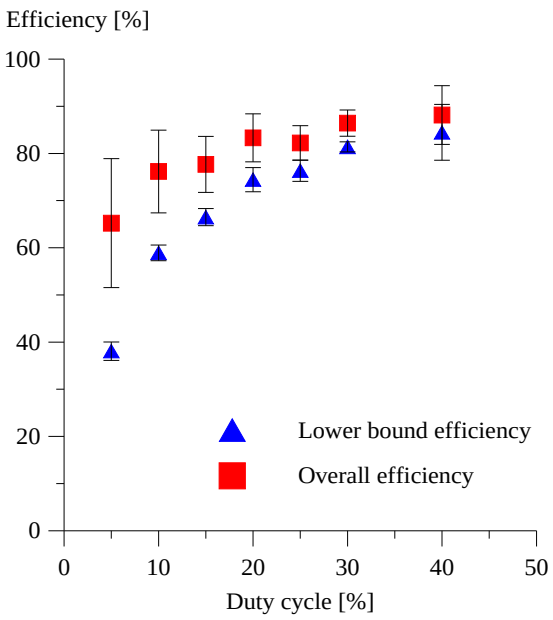


Fig. 8 Lower bound actuator efficiency and estimated overall actuator efficiency at the conditions of Fig. 7.

repetitive RF burst waveform is primarily controlled by the duty cycle, as expected.

Figure 7 shows time-averaged input DC power and time-averaged pulsed RF discharge power in a plasma actuator in a Mach 0.9 flow at a forcing frequency of 5 kHz vs. duty cycle. In these and all subsequent measurements, the actuator current was measured using a Tektronix current probe. RF discharge power was calculated as a mean value averaged over 5 consecutive RF bursts during the same run. Again, pulsed RF discharge power in Fig. 7 represents a lower bound value since it does not include energy coupled to the flow during first 4 μsec of the burst, which include resonance voltage increase (over up to 1-3 μsec, see Fig. 4) and breakdown. It can be seen that, as expected, the time-averaged discharge power increases approximately linearly with the duty cycle with good run-to-run reproducibility, showing that power during the current-limited stage in the burst remains about the same. At a forcing frequency of 5 kHz, pulsed RF discharge power is 11.6±0.3 W at 15% duty cycle and 46.7±3.2 W at 40% duty cycle.

Figure 8 shows the lower bound power conversion efficiency, i.e., the ratio of the time-averaged pulsed RF discharge power dissipated in the actuator and the input 400 V DC power of the RF plasma generator, for the same conditions as in Fig. 7. Thus, the power conversion efficiency represents the efficiency of the entire system, including the RF generator and the plasma actuator. At a forcing frequency of 5 kHz, lower bound efficiency increases from 38% at 5% duty cycle to 80-85% for 30% and 40% duty cycles. Figure 8 also shows the estimated overall power conversion efficiency, which includes both power coupled during repetitive breakdown, ≈ 0.4 mJ x 5 kHz ≈ 2 W, and during the current-limited mode. It can be seen that the overall efficiency variation with the duty cycle is less significant than that of the lower bound efficiency. Note that since the repetitive breakdown pulse power is basically independent of the duty cycle, its relative contribution to the overall RF discharge power decreases considerably at high duty cycles. For this reason, the overall efficiency at high duty cycles is close to the lower

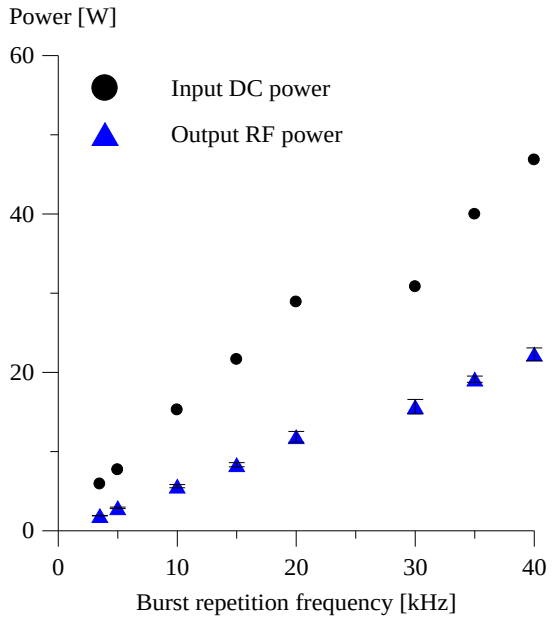


Fig. 9 Time-averaged input DC power and lower bound pulsed RF discharge power vs. burst repetition rate at the same burst duration of 10 μsec. at Mach 0.9 jet.

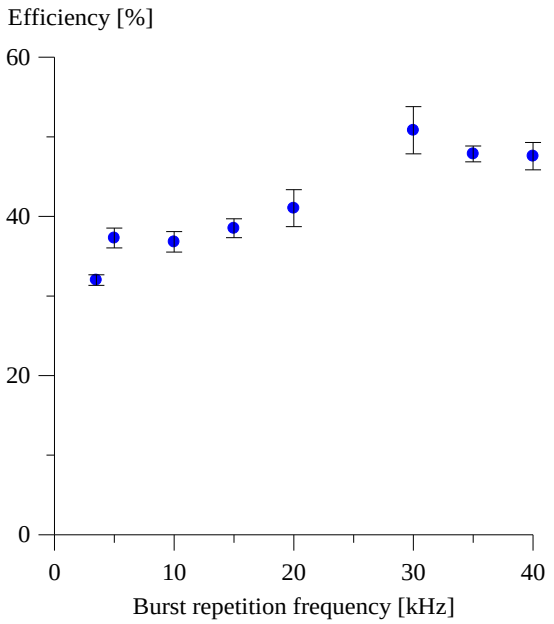


Fig. 10 Lower bound actuator efficiency at the conditions of Fig. 9.

bound efficiency and is estimated to be 87±6% at a 40% duty cycle (see Fig. 8). Similar measurements at a higher forcing frequency of 20 kHz, not shown here, yielded the overall efficiency of 80±5% for 30% and 40% duty cycles. In quiescent air, power conversion efficiencies in the breakdown mode and in the current-limited mode have been measured separately, giving 75% at a forcing frequency of 1 kHz and a duty cycle of 0.5% (breakdown mode) and 92% at a forcing frequency of 20 kHz and 20% duty cycle (current-limited mode), respectively. These results demonstrate that the use of DC / pulsed RF power conversion improves plasma actuator efficiency by approximately an order of magnitude compared to the pulsed DC actuators used in our previous work (Samimy et al. 2004; Samimy et al. 2007a; Samimy et al. 2007b; Utkin et al. 2007), from 5-10% to 80-90%.

Figures 9 and 10 show input DC power, lower bound pulsed RF discharge power, and lower bound efficiency vs. burst repetition rate, for the constant burst duration of 10 µsec. In these figures, breakdown pulse power is again not taken into account. Time averaging of the discharge power in the current limited mode was done for 4 µsec < t < 10 µsec, to exclude breakdown pulse power. It can be seen that the discharge power increases approximately linearly with the forcing frequency, as expected. As the forcing frequency increases from 3.5 kHz to 40 kHz, the lower bound efficiency somewhat increases, from about 30% to 45-50%. This effect is likely due to breakdown voltage reduction at high forcing frequencies, at which the plasma does not fully decay between the bursts. This also reduces breakdown delay time, from 1.3 µsec at 3.5 kHz to 0.8 µsec at 40 kHz and increases the quasi steady state, current-limited discharge duration.

Note that the low bound efficiency plotted in Fig. 10 would considerably increase at longer burst durations (higher duty cycles) or if the repetitive pulse breakdown power is taken

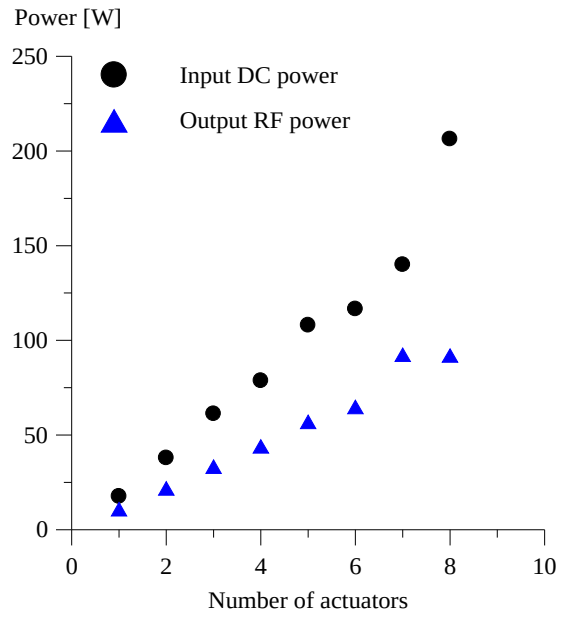


Fig. 11 Input DC power and RF discharge power dependence on the number of actuators operating together at a forcing frequency of 5 kHz, duty cycle of 15%, and m=0 in Mach 0.9 jet.

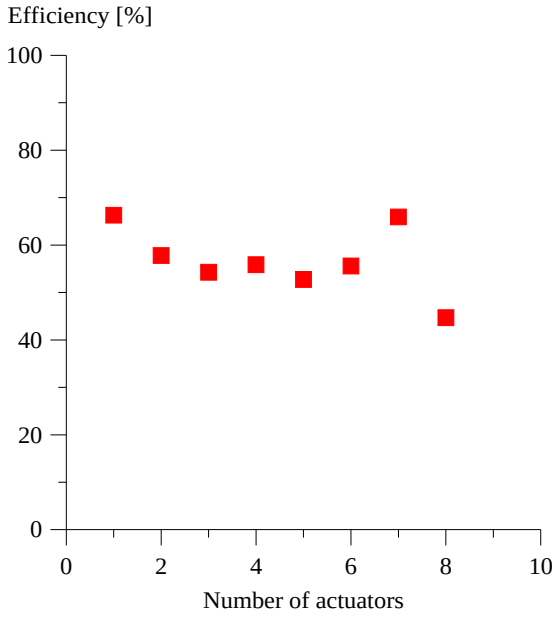


Fig. 12 Lower bound DC/RF power conversion efficiency at the conditions of Fig. 11.

into account, as can be seen in Fig. 8 (5% duty cycle data points in Figs. 7 and 8 corresponds to the burst duration of 10 μsec).

Figures 11 and 12 show the effect of multi-channel operation on actuator power and efficiency. Figure 11 plots input DC power dependence on the number of actuators, *N*, at m=0 (i.e. when all actuators are fired simultaneously), forcing frequency of 5 kHz, and a duty cycle of 15% (burst duration 30 μsec). It can be seen that the input power increases linearly up to the *N*=7. For *N*=8 (when all 8 actuators are operating), the input power is somewhat higher (by about 25% compared to the extrapolated linear fit). At these conditions, noticeable fluctuations of input DC current have also been detected. This behavior is most likely due to interference between arc discharges produced by individual actuators located close to each other (center-to-center distance between electrodes of two adjacent actuators is 6 mm, for the electrode gap of 4 mm in each actuator). Figure 11 also plots current-limited RF discharge power measured in one of the actuators at these conditions, multiplied by the number of actuators in operation. Finally, Figure 12 shows the lower bound efficiency calculated from the data of Fig. 11 (output current-limited RF discharge power over input DC power). It can be seen that the lower bound efficiency, which varies between 55% and 67% for *N*=1-7 is fairly weakly affected by the number of actuators in operation. We therefore conclude that cross-channel interference of individual pulsed RF discharges remains a relatively minor effect.

*3.2. Flow field and acoustic results*

In our previous flow control work using pulsed DC plasma actuators, it was shown that LAFPAs have significant control authority in a subsonic Mach 0.9 jet (Samimy et al. 2007a; Kim et al. 2009) and in a supersonic Mach 1.3 jet (Samimy et al. 2007b; Kim and Samimy 2009). In this section, flow control performance of pulsed RF plasma actuators, characterized in Section 3.1, is investigated in a 1 inch (2.54 cm) diameter Mach 0.9 circular jet and compared with that of pulsed DC actuators. The results using DC and RF actuators are compared at the same forcing frequencies, $f_F$ (i.e. DC pulse or RF burst repetition rate, respectively) and duty cycles, δ. The number of actuators for all results presented in this section is *N*=8.

Figure 13 compares ensemble-averaged streamwise velocity fields in a Mach 0.9 jet forced by pulsed DC and pulsed RF plasma actuators in a flapping mode (m= ±1) at three different forcing Strouhal numbers, $St_{DF}$ = 0.27, 0.32, and 1.09. The forcing Strouhal number is based on the forcing frequency, jet diameter, and jet exit velocity, $St_{DF} = f_F D/U_j$. Actuator duty cycles for these three cases are 3.8%, 4.4%, and 9.6%, respectively. Flapping mode was chosen since the effect of forcing in this mode has been shown to be most pronounced (Samimy et al. 2007b; Kim et al. 2009; Kim and Samimy 2009). DC forcing was produced using an 8-channel pulsed DC plasma generator used in our previous work (Samimy et al. 2007a; Samimy et al. 2007b; Utkin et al. 2007). Note that time-averaged DC and RF actuator discharge powers in a Mach 0.9 jet are very close to each other, approximately ~ 100·δ W, where δ is the duty cycle (Adamovich et al. 2009). This implies that the electrical power dissipated in the flow is nearly the same for both DC and RF forcing.

Comparing baseline velocity fields in Figures 13a and 13b, it can be seen that spreading of baseline (unforced) jets exhibits some difference since the nozzle used with RF actuators has a different (more gradual) converging section profile, compared to the nozzle used with DC actuators. At $St_{DF}$ = 0.27 and 0.32, close to the jet column (preferred mode) instability Strouhal number, both DC and RF actuator forcing dramatically enhance jet spreading (see Fig. 13c-f). At these forcing Strouhal numbers, the jet potential core length is also significantly reduced compared to the baseline. However, jet spreading at a higher Strouhal number, $St_{DF}$ =1.09 (see

Fig. 13g,h) is similar to the respective baseline cases (a,b), suggesting that forcing at these conditions is not as effective as at Strouhal numbers close to the jet column instability frequency. The potential core length at these conditions also does not show significant change. Additional results showing the effect of forcing Strouhal number in a Mach 0.9 jet forced by DC actuators at m= ±1 in greater detail can be found in Samimy et al. (2007a) and Kim et al. (2009). The results of Fig. 13, as well as additional results which are not presented here demonstrate that the effect of forcing using RF actuators is very similar to that by DC actuators, in a wide range of forcing Strouhal numbers.

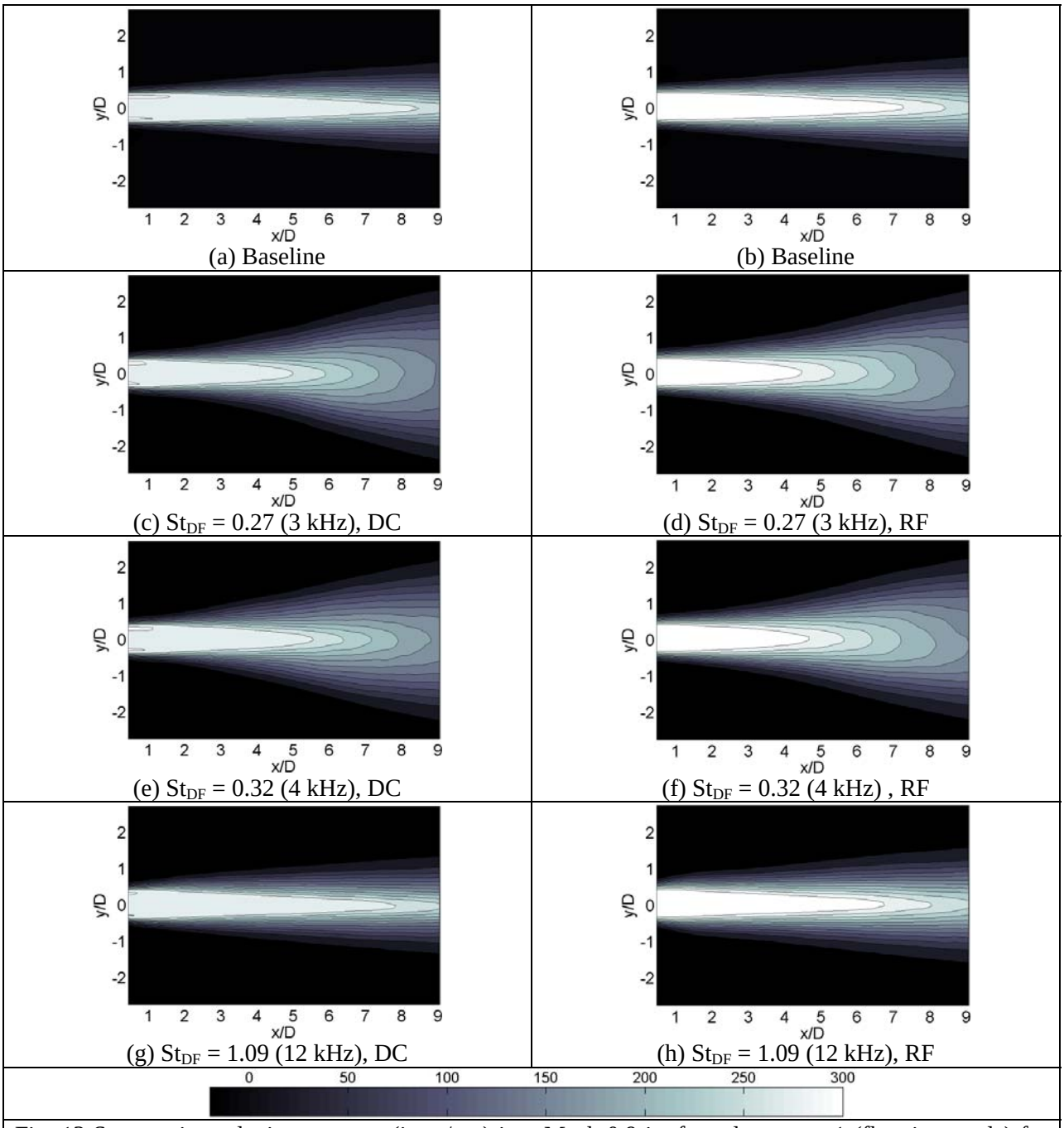


(a) Baseline (b) Baseline

(c) $St_{DF}$ = 0.27 (3 kHz), DC (d) $St_{DF}$ = 0.27 (3 kHz), RF

(e) $St_{DF}$ = 0.32 (4 kHz), DC (f) $St_{DF}$ = 0.32 (4 kHz) , RF

(g) $St_{DF}$ = 1.09 (12 kHz), DC (h) $St_{DF}$ = 1.09 (12 kHz), RF

Fig. 13 Streamwise velocity contours (in m/sec) in a Mach 0.9 jet forced at m = ±1 (flapping mode) for various forcing Strouhal numbers. Left column, for DC actuators; right column, for RF actuators.

More quantitative comparison of DC and RF actuator performance is shown in Fig. 14 for three different azimuthal modes, m=0 (axisymmetric), m=1 (first helical), and m= ±1 (flapping). Mach number decay on the jet centerline is used as quantitative indicators of jet spreading (Kim et al. 2009; Kim and Samimy 2009). The cases shown in Fig. 14 are at the optimal forcing Strouhal numbers, when the jet spreading is maximum, $St_{DF}$ = 0.36, 0.27, and 0.27 for m = 0, 1, and ±1, respectively. As discussed above, the centerline Mach number for the baseline jets is different since the nozzles used with DC and RF actuators are not the same. Discussion of the effect of nozzle profile is beyond the scope of the present research, which focuses on DC and RF actuator performance comparison, i.e. on a relative change from a respective baseline jet.

In the axisymmetric mode (at m=0), the relative enhancement in centerline Mach number decay by both types of actuators at the optimal forcing Strouhal number, $St_{DF}$=0.36, is about the same (see Fig. 14a). The potential core length is shortened by about two jet diameters (2D), for both DC and RF forcing cases.

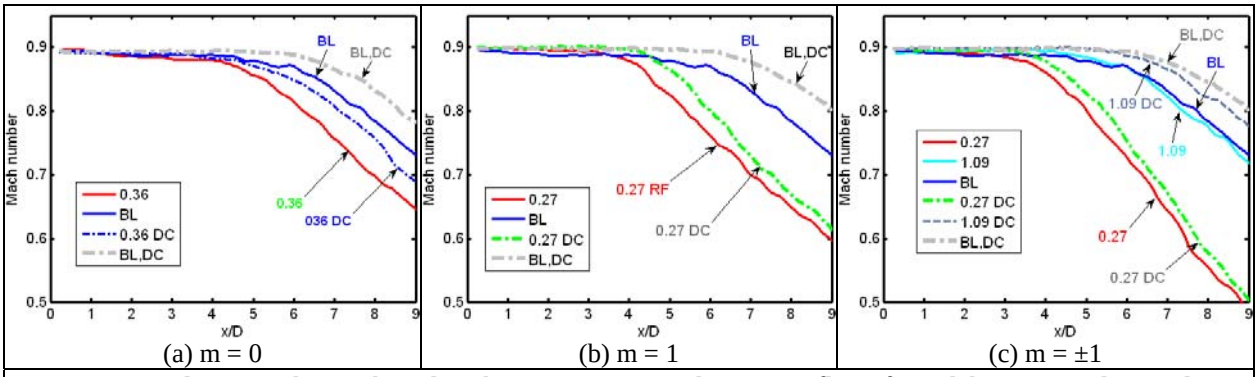


(a) m = 0 (b) m = 1 (c) m = ±1

Fig. 14 Centerline Mach number distributions in a Mach 0.9 jet flow forced by DC and RF plasma actuators. Text labels indicate forcing Strouhal number; labels without "DC" tag correspond to RF forcing cases.

In the first helical mode (at m=1), centerline Mach number distributions in jets forced with DC and RF actuators are very close to each other beyond x/D > 6 (see Fig. 14b), although the baseline jets show moderate disparity. In both DC and RF actuator forcing, the potential core length is reduced by about 2D, similar to that of m=0 case.

In the flapping mode (m= ±1), the centerline Mach number decay was dramatically increased at the optimal forcing Strouhal number of $St_{DF}$=0.27, as shown in Fig. 14c. At these conditions, the centerline Mach number profiles for DC and RF actuator forcing are similar. In both cases, the potential core length is reduced by approximately 3D. Figures 14c also shows additional results for DC and RF actuator forcing in the flapping mode at a higher Strouhal number, $St_{DF}$=1.09, corresponding to the two cases shown in Figs. 13g,h. At these conditions, the centerline Mach number decay rate is slightly enhanced by both DC and RF actuator forcing (see Fig. 14c).

DC and RF actuator effect on jet spreading (not shown here) shows noticeable difference for m=0 and m=1, while DC and RF forcing results for m= ±1 are in very close agreement. A possible cause for this difference is using nozzles with different converging section profiles. Another possible reason is significant difference in the plasma temperatures, 300-1300° C in DC

actuators vs. 1200-2500° C in RF actuators (Adamovich et al. 2009). At this point, the cause for the difference between DC and RF forcing at m=0 and m=1 remains an open question.

From Figs. 13-14, it can be seen that significant effect of RF plasma actuators on the flow is produced at very low input power. Time-averaged input electrical power required to operate all 8 pulsed RF plasma actuators in the first helical mode at duty cycles of 4-10% is approximately 50-125 W, compared to the flow power of 58 kW (stagnation enthalpy flux).

Conditionally-averaged Galilean streamlines, superimposed on the streamwise velocity component, are used to investigate the effect of actuator forcing on generation of large-scale flow structures. Galilean streamlines are streamlines in a coordinate system moving with the convective velocity of large-scale structures, rendering such structures stationary and visible, with either spiraled or closed shape streamlines. The conditionally-averaged images are similar to those that can be obtained from phase-locked images relative to the control signal. Two-dimensional cross-correlation to a reference image was calculated for all 700 instantaneous images. Approximately 30 to 40 instantaneous images, highly correlated to the reference image,

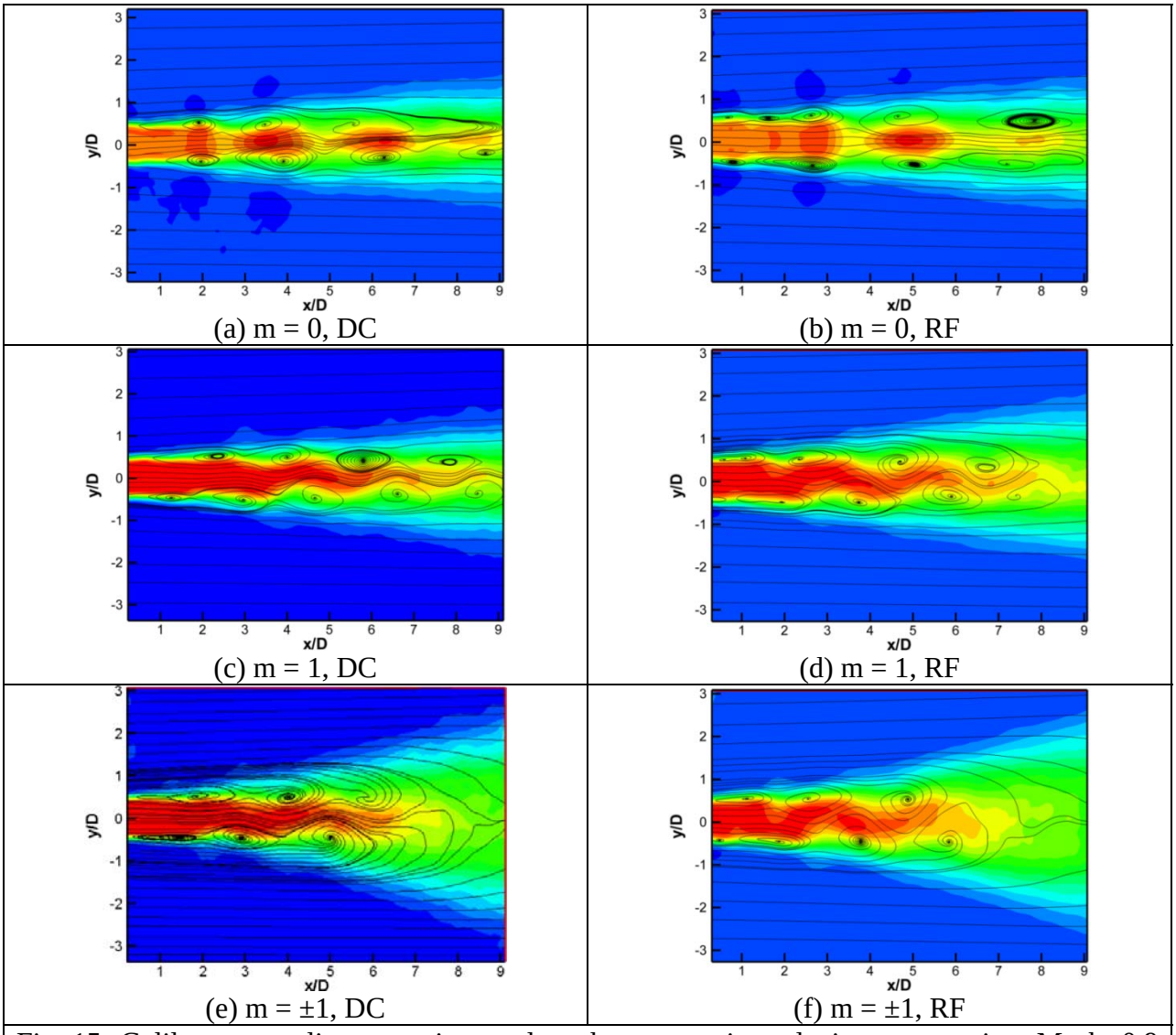


(a) m = 0, DC (b) m = 0, RF

(c) m = 1, DC (d) m = 1, RF

(e) m = ±1, DC (f) m = ±1, RF

Fig. 15 Galilean streamlines superimposed on the streamwise velocity contours in a Mach 0.9 jet at $St_{DF}$=0.32. Left column, for DC actuators; right column, for RF actuators.

were averaged to obtain a conditionally-averaged image. Details of conditional averaging and Galilean decomposition, including calculations of convection velocity, can be found in Kim et al. (2009).

Conditionally-averaged Galilean streamlines for m = 0, 1, and ±1 are shown in Fig. 15 for Strouhal number of $St_{DF}$ = 0.32, which is close to the optimal forcing Strouhal number for these azimuthal modes. In our previous work (Kim et al. 2009; Kim and Samimy 2009), the pattern and size of large-scale structures generated in the flow were shown to play an important role in jet development. When the flow is forced with the axisymmetric mode (m=0), the vortical structures generated in the top and bottom of the flow are in phase since they are ring vortices. From Fig. 15 (a & b), it can be seen that the structures generated by both DC and RF actuators are periodic in space and well organized. The pattern and size of these structures in these two cases appear similar, suggesting that both DC and RF actuators are effectively and similarly forcing the jet. These large-scale, well-organized structures are responsible for the more rapid centerline Mach number decay observed in Figs. 13 and 14.

When the flow is forced with first helical (m=1) and flapping (m=±1) modes, the structures generated in top and bottom shear layers are out of phase. They are also periodic and well-organized, with dimensions and patterns similar with DC and RF actuators. The pattern of large-scale structures at m= ±1 is very similar to that at m= 1. At m= ±1, the structures are larger in the spanwise direction and thus more energetic than those at m = 1. As a result, the jet plume is more undulating for m= ±1 than for m= 1. The enhanced undulation of the jet plume by large-scale energetic structures is responsible for the significantly reduced jet potential core length observed in Figs. 13 and 14.

For all forcing modes presented, the pattern and dimensions of structures generated by both DC and RF actuators are similar, suggesting that the effect of both types of actuators on manipulation of flow instabilities are also similar. Based on the flow field results discussed so far, it appears that the performance of RF actuators used for flow control is essentially the same as that of DC actuators.

The performance of DC and RF actuators used for noise mitigation in the Mach 0.9 jet is compared using far-field Overall Sound Pressure Level (OASPL). Figure 16 shows the change in OASPL (ΔOASPL) relative to the respective baseline with forcing Strouhal number ranging from $St_{DF}$ =0.1 to 5 (forcing frequency $f_F$ =1-60 kHz) for different forcing azimuthal modes, m= 0-3. The duty cycle was increased linearly with forcing Strouhal number to avoid misfire, as discussed in detail in Kim et al. (2009). The far-field noise was measured at two polar angles of $30^0$ and $90^0$ relative to the jet axis, as discussed in Section 2. Our previous acoustic results, obtained using 8 DC actuators (Samimy et al. 2007a) are shown in Fig. 16a,b to compare with the present results obtained using 8 RF actuators (see Fig. 16c,d).

At $30^0$ polar angle, the trend of ΔOASPL measured using DC actuators (Fig. 16a) is very similar to that obtained using RF actuators (Fig. 16c). At low $St_{DF}$ values, the OASPL increased for both DC and RF actuator forcing. As shown in Fig. 15, large, well-organized structures were generated by both types of actuators at low forcing Strouhal number of $St_{DF}$ = 0.32. Dynamics of these large-scale structures are responsible for the increase in OASPL. At high $St_{DF}$ values, there is a moderate reduction in OASPL. The largest OASPL reduction using DC actuators is about 1.2 dB, compared to approximately 1.5 dB obtained using RF actuators (see Fig. 16a,c). As discussed earlier, the mean flow field at these high $St_{DF}$ values does not exhibit significant change from the baseline.

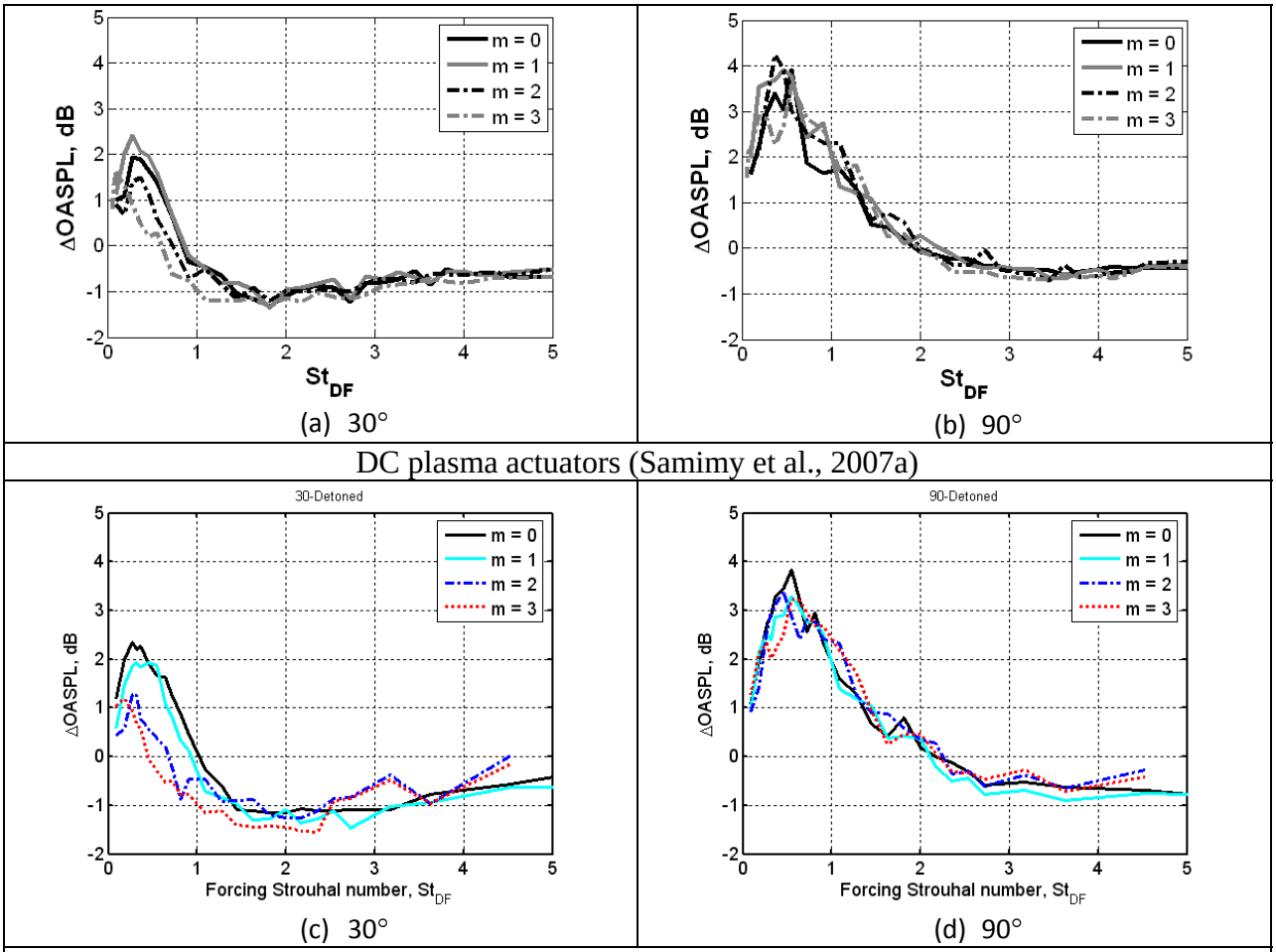


Fig. 16 Variation of ΔOASPL with forcing Strouhal number for different azimuthal forcing modes. (a,b) for DC forcing; (c,d) for RF forcing

At $90^0$ polar angle, ΔOASPL is less dependent on the azimuthal mode, and the trend of ΔOASPL obtained using DC actuators remains similar to that measured using RF actuators (see Fig. 16b,d). As was observed at 30˚ polar angle, the noise level is significantly increased at low forcing Strouhal numbers. At high $St_{DF}$ values, a moderate reduction of 0.6 to 0.8 dB is observed. These results suggest that the effect of DC and RF plasma actuators on the acoustic field is essentially the same.

## 4. Summary

The present work characterizes a new custom-designed 8-channel pulsed RF plasma generator, and compares its performance with that of a previously designed and used 8-channel DC plasma generator in flow and noise control of a Mach 0.9 circular jet with the Reynolds number based on jet diameter of approximately 623,000. The new plasma generator converts low voltage DC input into RF output with peak voltage rapidly increasing until breakdown occurs in the load (plasma actuator). After breakdown, RF voltage is reduced by more than an order of magnitude as the discharge reaches quasi-steady state. In contrast to the DC plasma generator, the RF plasma generator does not contain dissipative circuit elements such as ballast resistors.

The overall power conversion efficiency of the pulsed RF actuator, defined as the ratio of the output pulsed RF discharge power and the input low-voltage DC power, is up to 80-85%. Input electrical power consumption is 12-25 W per actuator operating at 10-20% duty cycle. The new plasma generator operates in a wide range of burst repetition rates (forcing frequencies) (from a few Hz to a few tens of kHz) and duty cycles (from below 1% to 50%), with independent burst repetition rate, duty cycle, and phase control of individual actuators. No significant EMI noise, electrode erosion, or interference between the actuators has been detected during multi-channel operation.

The performance of pulsed RF actuators for flow and noise control in a Mach 0.9 axisymmetric jet has been studied using PIV and acoustic measurements. The results show that forcing with both DC and RF actuators reduces the potential core length, compared to respective baseline cases. The effect is most pronounced at forcing Strouhal numbers of 0.27-0.36 ($f_F$=3-4 kHz), close to the jet column (preferred mode) instability frequency. At high forcing Strouhal numbers, the jet centerline Mach number is similar to that of the baseline jet, demonstrating that actuator forcing is most effective when the forcing frequency is close to the jet column instability frequency. As apparent from comparison of streamwise velocity contours and Galilean streamlines, quantitative effect of DC and RF forcing on the flow field at the same Strouhal number and the same azimuthal mode is very similar. In both cases, repetitive forcing generates well organized, large-scale vortical structures in the flow, similar to large-scale coherent structures in low-speed and lower Reynolds numbers jets. Significant effect on the flow is produced at low plasma power, approximately 50-125 W for 8 actuators, which is less than 0.5% of the flow power. Acoustic measurements demonstrated that change in the overall sound pressure level when using DC and RF plasma actuators exhibits essentially the same characteristics, showing noise increase at relatively low Strouhal numbers, $St_{DF} < 1$, and noise reduction up to 1.2 - 1.5 dB at higher Strouhal numbers, $St_{DF} > 1$-2, compared to baseline.

Scaling of the new 8-channel pulsed RF plasma generator unit to a system with a larger number of channels is straightforward. Assuming that the number of actuators needed for effective flow control scales linearly with the jet diameter, approximately 96 actuators would be necessary for control of a 12 inch diameter jet. A 96-channel generator would incorporate 12 such units controlled by a common programmable control board and would use the same 500 V, 20 A Magna Power DC power supply as used in the present work. Operating 96 plasma actuators in the first helical mode at a duty cycle of 10%, which was typically used in our previous and present flow control experiments would require approximately 1.2 kW input DC power (400 V, 3 A). The results of the present work demonstrate a practical approach to developing highly energy efficient plasma flow control systems scalable to a larger facility. Further experiments in larger cross section area flows are necessary to determine scalability of the LAFPA technology.

## 5. Acknowledgments

The support of NAVAIR (with Dr. John Spyropoulos) through an SBIR program with Spectral Energies and NASA (with Dr. James Bridges and Mr. Cliff Brown) is greatly appreciated. The authors also acknowledge the contribution of Sivaram Gogineni of Spectral Energies.

## References


Adamovich, I.V., Choi, I., Jiang, N., Kim, J.-H., Keshav. S., Lempert, W.R., Mintusov, E., Nishihara, M., Samimy, M., and Uddi, M. (2009), "Plasma Assisted Ignition and High-Speed Flow Control: Non-Thermal and Thermal Effects", Plasma Sources Science and Technology, vol. 18, p. 034018

Adelgren, R.G., Yan, H., Elliott, G.S., Knight, D.D., Beutner, T., and Zheltovodov, A.A. (2005), "Control of Edney IV Interaction by Pulsed Laser Energy Deposition", AIAA Journal, vol. 43, pp. 256-259

Adelgren, R.G., Elliott, G.S., Crawford, J.B., Carter, C.D., Donbar, J.M., and Grosjean, D.F. (2005), "Axisymmetric Jet Shear-Layer Excitation by Laser Energy and Electric Arc Discharges", AIAA Journal, vol. 43, pp. 776-791

Brown, G.L., and Roshko, A., "On Density Effects and Large Structure in Turbulent Mixing Layers" (1974), Journal of Fluid Mechanics, vol. 64, pp. 715–816

Cohen, J., and Wygnanski, I. (1987), "The Evolution of Instabilities in the Axisymmetric Jet. Part 1. The Linear Growth of Disturbances Near the Nozzle," Journal of Fluid Mechanics, vol. 176, pp.191-219

Crow, S.C., and Champagne, F.H. (1971), "Orderly Structure in Jet Turbulences," Journal of Fluid Mechanics, vol. 48, pp. 547-591

Hussain, F., and Zaman, K. (1981), "The Preferred Mode of the Axisymmetric Jet," Journal of Fluid Mechanics, vol. 110, pp. 39-71

Kim, J.-H., Kastner, J., and Samimy, M. (2009), "Active Control of High Subsonic Jets," AIAA Journal, vol. 47, No. 1, pp. 116-128

Kim, J.-H., and Samimy, M. (2009), "Effects of Active Control on Flow Structure in a High Reynolds Number Supersonic Jet," accepted for publication in International Journal of Flow Control

Leonov, S.B., and Yarantsev, D.A. (2008), "Near-Surface Electrical Discharge in Supersonic Airflow: Properties and Flow Control", Journal of Propulsion and Power, vol. 24, pp. 1168-1181

Moreau, E. (2007), "Airflow Control by Non-thermal Plasma Actuators", Journal of Physics D: Applied Physics, vol. 40, pp. 605-636

Roupassov, D.V., Nikipelov, A.A., Nudnova, M.M., and Starikovskii, A.Yu. (2009), "Flow Separation Control by Plasma Actuator with Nanosecond Pulse Periodic Discharge", AIAA Journal, vol. 47, pp. 168-185

Samimy, M., Adamovich, I., Webb, B., Kastner, J., Hileman, J., Keshav, S., and Palm, P. (2004), "Development and Characterization of Plasma Actuators for High Speed Jet Control", Experiments in Fluids, vol. 37, No. 4, pp. 577-588

Samimy, M., Kastner, J., Kim, J.-H., Utkin, Y., Adamovich, I., and Brown C. (2006), "Flow and Noise Control in High Speed and High Reynolds Number Jets Using Plasma Actuators", AIAA Paper 2006-2846, 37th AIAA Plasmadynamics and Lasers Conference, June 2006, San Francisco, CA

Samimy, M., Kim, J.-H., Kastner, J., Adamovich, I., and Utkin, Y. (2007a), “Active Control of a Mach 0.9 High Reynolds Number Jet for Noise Mitigation Using Plasma Actuators”, AIAA Journal, vol. 45, No. 4, pp. 890-901

Samimy, M., Kim, J.-H., Kastner, J., Adamovich, I., and Utkin, Y. (2007b), “Active Control of High-speed and High Reynolds Number Jets Using Plasma Actuators”, Journal of Fluid Mechanics, vol. 578, pp. 305-330

Utkin, Y.G., Keshav, S., Kim, J.-H., Kastner, J., Adamovich, I.V., and Samimy, M. (2007), “Development and Use of Localized Arc Filament Plasma Actuators For High-speed Flow Control”, Journal of Physics D: Applied Physics, vol. 40, pp. 685-694

Zaman, K.B.M.Q., and Hussain, A.K.M.F. (1982), “Turbulence Suppression in Free Shear Flows by Controlled Excitation”, Journal of Fluid Mechanics, vol. 103, pp. 133-159